Plasma characteristics in the backflow region of ion thruster plumes using kinetic and Boltzmann models

IEPC-2019-A-367

Presented at the 36th International Electric Propulsion Conference
University of Vienna, Austria
September 15-20, 2019

Nakul Nuwal* and Deborah Levin†
University of Illinois Urbana-Champaign, Urbana, IL, 61801, USA

Plasma surface interactions are an important aspect of spacecraft design. The spacecraft solar panel surfaces present in the backflow region of the plume can acquire a negative potential with respect to the plume, attracting the slow moving charge exchange ions created in the core plume region. The ions accelerating towards the surface can cause surface sputtering of the protective coating present on the solar panels. In this work, we present a three-dimensional fully-kinetic numerical study of ion thruster plume plasma interactions with spacecraft surfaces where all species are considered as particles and their individual kinetics is resolved. A time explicit PIC-DSMC numerical technique is used to perform plasma simulations using a hybrid MPI-GPU code, CHAOS, which has been modified to include the effects of the surfaces present in the backflow region. Here, we present the plasma macro-parameters, such as ion and electron densities, and the kinetic parameters such as ion energy distribution and plasma-sheath thickness near the surface from our numerical simulations. Finally, we estimate the surface erosion of solar panel surface using the kinetic model results and surface yield empirical relations, and relate it with the plasma sheath thickness found near the solar panel surface.

*Graduate student, Aerospace engineering University of Illinois Urbana-Champaign, and nuwal2@illinois.edu.
†Professor, Aerospace engineering University of Illinois Urbana-Champaign, and deblevin@illinois.edu.

I. Introduction

Electric propulsion (EP) devices are widely used in space for orbit correction and station keeping of the satellites.[1] Their high specific impulse makes them very efficient for propulsion in space where the mass of propellant carried for the mission is limited. These devices, however, provide a small propulsion force of the order of 5 mN for a long periods of time during their operation in space.[2] The xenon gas is ionized and then accelerated through the electrostatically charged grids to thruster exit velocities of about 40 km/s to create propulsion. Since these devices operate for a long time during a space mission, their cumulative effect on the spacecraft surfaces is crucial to the mission. The plasma plume generated by ion thrusters consists of high-speed ions, neutralizing electrons, and slow moving neutrals of which the fast moving ions are mainly responsible for the thrust produced and account for about 5 % of the total mass flux from the thruster, while the rest of the mass is composed of neutrals which come from the thruster exit at a much lower speed compared to the ions. Near the thruster exit, where the number densities are high enough for ion-neutral collisions to occur, slow moving charge exchanged (CEX) ions and fast moving neutrals are created.[3] The CEX ions have lower kinetic energies than the beam ions, but they can be accelerated towards the backflow surfaces with sufficiently high energy to cause sputtering damage on the solar cell array, affecting its longevity and performance. In addition, a hollow cathode emits electrons to neutralize the plasma plume which interact with the spacecraft surfaces to generate backflow electric fields hence affecting the charge exchange ion plasma behavior in the backflow region.[4]

Numerically, it is often hard to quantify and predict the near thruster plasma behavior over the life-time of a mission because of multiple time and length scales involved in the plume and backflow region due to the presence of gas species with different molecular masses and mobility. The numerical studies of Roy et. al[5] show good agreement in the core plume region, with ground based experiments, using a Boltzmann approximation for electron modeling, but do not include the effect of surfaces in the backflow region. The Boltzmann model assumes a constant electron temperature for the whole domain with quasi-neutrality assumed at every point. This model does not model the electron temperature variation along the plume as it expands, and is inaccurate outside the plume regions where quasi-neutrality is not a valid assumption. The majority of other plume plasma studies[6,7] treat electrons as a fluid medium and ions as particles. Previous work by Cichoki et.al. and Taccogna et. al[8] used a polytropic electron expansion model for ion plume expansion with a constant adiabatic coefficient. All these models exclude some important physical aspects of plume plasma, such as electron trapping by the ion plume and plasma sheath formation near the spacecraft surfaces. This merits the numerical resolution of electron physics in a plume plasma using a kinetic approach.

A collisionless three dimensional plume plasma has been modelled using a fully kinetic

PIC code, CHAOS, in Jambunathan et.al[9] and the thermal properties of electrons and electron trapping by the plume were found consistent with the other studies by Hu et al.[10–12] and Usui et al.,[13] who used a kinetic model in a two dimensional numerical domain. A more recent work[14] added the ion neutral particle collisions using DSMC model to the kinetic PIC to model the charge exchange ion plasma in the regions near the plume, but excluded a detailed model for the spacecraft solar panel surfaces present in the backflow region. In the current work, we use the code CHAOS[9,15] modified to include the spacecraft surface interactions with the plume plasma in the backflow region.

II. Methodology

A Particle-in-cell, Direct Simulation Monte carlo (PIC-DSMC) numerical technique is used for modeling the electric field and collisions in the domain, respectively. Since numerical calculations involve multiple orders of variation in length scales, unstructured octree forest of trees (FOTs)[15] grids are used for performing electric field and collision calculations for this work. A number of simulations were performed to understand kinetic effects of plume plasma interactions with spacecraft surfaces. The case using the kinetic model is designated as 'Case A' and the case using the Boltzmann model is named as 'Case B'.

A. Particle in cell (PIC)

An explicit particle-in-cell (PIC) technique is used to solve for electric field.[9] The electric potential is solved for using Poisson's equation, which is solved numerically with a finite volume method,[9,15] and based on the electric field, ions and electrons are moved every time-step in that order. Since electrons move at a time-scale of the electron plasma frequency, the time-step used for the simulations is such that $\omega_{pe}\Delta t < 0.1$, ω_{pe} being the plasma frequency, and the electric field is computed at every time-step. Also, since the effects of local charge extend to a length scale on the order of local Debye length, the grid used for solving Poisson's equation, E-FOT, satisfies the grid refinement criteria of cell size being smaller than the local Debye length.[9,16] Additionally, a charge and energy conserving boundary condition has been used to stabilize the plume once the plume-front leaves the domain.[17] The spacecraft solar panel surface in the backflow region is shown in Figs. 1 and 2. To emulate the spatial potential drop across solar panel surfaces, a Dirichlet boundary has been used at the solar panel surface shown in blue color in Fig. 2.

1. *Solar panel surface boundary*

The solar panel surfaces in space typically have a potential drop of 1000's of volts across their length with respect to the spacecraft ground as the solar cells are electrically connected in series. To model a scenario where solar panels and ion thrusters are operating simultaneously, a Dirichlet boundary condition is applied on the solar panel surface for Case A, and a potential drop of 60 V is assigned along the solar panel span of 0.275 m and the spacecraft ground is considered to lie at 0 V.

2. *Boltzmann model*

To compare with the kinetic simulation, we have used a Boltzmann electron temperature model as described in Korkut et. al.[3] The electric potential due to the plume plasma using Boltzmann model is given by,

$$\phi_{\mathrm{pl}} = \phi_{\mathrm{ref}} + \frac{kT_e}{e} \log\left(\frac{n_e}{n_0}\right), \tag{1}$$

where ϕ_{pl} is potential due to plume plasma, ϕ_{ref} is the reference potential, k is Boltzmann constant, T_e is reference electron temperature, e is the electron elementary charge, n_e is the electron number density and n_0 is the reference electron number density. The plasma is assumed to be quasi-neutral in the whole domain, $n_e = n_i$, where n_i is the ion number density. Additionally, because there is a negative potential surface present in the backflow region, the external field due to the voltage drop across the solar cell array is calculated in the domain by solving,

$$\nabla^2 \phi_{\mathrm{ext}} = 0, \tag{2}$$

with the solar panel surfaces assigned a spanwise varying potential with a linear potential drop of 60 V. The superposition technique is used to obtain total electric potential,[7]

$$\phi = \phi_{\mathrm{pl}} + \phi_{\mathrm{ext}}. \tag{3}$$

For the model to be valid, the E-Octree should have a cell size (Δx) of the order of the local Debye length(λ_{D}) and since there are no electron particles modeled in the domain, a two orders of magnitude higher time-step may be used for this case.

B. Direct Simulation Monte Carlo (DSMC)

We have used the no-time counter (NTC) scheme[18] to model collisions between xenon atoms and ions based on their collision cross-sections.[3] Since length scale for collisions or the mean free path is much larger compared to plasma length scale or the Debye length, a different coarser grid, C-FOT, is used for modeling collisions.[9,15] The collision time-scale is about two orders of magnitude greater than electron plasma frequency time-scale, therefore collisions are performed about 100 times less frequently than electric field calculations in the simulation. Also, because the time-scale difference is large, use of different time-steps does not affect the time accuracy of simulations.

C. Surface sputtering

The charge exchange (CEX) ions from the plume are incident on the surface of solar panels in the backflow region of the thruster plume. The number of particles of the target material removed by an incident ion from the target surface is known as surface yield. As per empirical models given in Yamamura et.al.,[19] the surface yield of an ion on a surface, Y, depends on incident ion energy, E_i and the angle of incidence θ_i. An empirical relation of Bohdansky et. al.[20] is used to calculate yield for every incident ion. Since each computational particle in DSMC represents a finite, F_num, number of particles, each computational particle will remove $F_\mathrm{num} Y(E_\mathrm{i}, \theta_\mathrm{i})$ number of target element atoms from the surface. Based on the material number density of the target element, sputter-yield information and the number of particles incident, the surface recession rate (m/s) at a point on the surface can be calculated by

$$S(\mathrm{m/s}) = \frac{f_{\mathrm{Xe+}} F_\mathrm{num} Y(E_\mathrm{i}, \theta_\mathrm{i})}{n_\mathrm{T}}, \tag{4}$$

where, $f_{\mathrm{Xe+}}$ is the number of computational Xe^+ ions incident at the point on the surface per m^2 per second and n_T is the number density of the target element (atoms/volume).

III. Results and Discussion

The numerical simulations are performed in a computational domain of size $(0.8 \times 0.8 \times 0.4)$ m shown in Fig. 1 with the thruster exit at (0.4, 0.4, 0.1) m as marked in red with co-located ion and electron sources. A sectional view of the domain is shown in Fig. 2. The ions enter the domain from the thruster exit with a Gaussian beam width of half angle of 12$^\mathrm{o}$ and a bulk velocity of 40 km/s. Case A was performed using 32 GPU's in CUDA environment and took 144 hours to finish. The following sections provide a detailed description of the numerical cases performed for this work.

The plasma plume forms when electron and ion particles enter the domain from the same location with inlet paramters shown in Fig. 1. Since ions have a higher mass than electrons, the plume front, i.e. the point along the plume axis till which the quasi-neutrality is satisfied, moves at a speed of ions, i.e. 40 km/s in the z direction. However, because of their lower mass, the electrons quickly spread throughout the domain. The plume front for Case A reaches the end of the domain at z = 0.4 m in about 27,000 time-steps (7.56 μs), i.e. $\omega_{pe}t = 1,350$, for a time-step PIC $\Delta t = 2.8 \times 10^{-10}$ s, and the electric field reaches steady state in about 100,000 time-steps (28 μs), i.e. $\omega_{pe}t = 5,000$, when the electric potential in the backflow region does not vary by more than 4 V with time. The electric field is sampled for about 50,000 time-steps in the PIC calculations, after reaching steady state to reduce statistical errors. The charge exchange ion collisions are performed every 100 time-steps making the DSMC time-step 100 times larger than that of the PIC time-step. Since the charge exchange ion number density is about three orders of magnitude smaller than the plume ion number density, these ions are inconsequential in forming the electric field in the domain. Hence, after a time that the electric field is sufficiently time-sampled, only the DSMC calculations to model charged-neutral particle collisions are performed to save the computational cost of solving Poisson's equation at every time step. The DSMC calculations reach steady state when the CEX ions start leaving the domain from the domain boundaries or are neutralized on the solar panel surface. The DSMC macro-parameters are sampled for an additional 50,000 DSMC times during which the electric field calculations are not performed, electrons are not moved, only the neutral-neutral and neutral-ion collisions are modelled, and neutrals and ions are moved subject to the steady state electric field.

The presence of solar panel surfaces in the backflow region changes the electric in the region outside the plume. A comparison of Figs. 3(a) and 3(b) shows that while the core plume electric potential compares well for both YZ and XZ planes, the effect of the solar panel surface, shown in Fig. 3(c), is visible on YZ plane section where the biased surface lies at z = 0 m. The electric field affects the electrons more than the ions in a single time-step because of their high mobility. The electron number density in the mid-plane (x = 0.4 m) of the domain, shown in Fig. 4(a), is very low near the solar panel surface at z = 0.0 m which repels electrons in the plume plasma. Since E_z is more negative when we move farther from thruster exit in the spanwise direction, y direction, shown by the potential drop in Fig. 4(c), the solar panel surface repels the electrons and the region devoid of electron particles increases in thickness. This region is termed as an 'ion plasma sheath'.

We define the plasma sheath thickness[21] as the distance from a point on the surface out to where the local electron number density is at least two times smaller than the local ion number density as shown in Fig. 8(a) where the electron number density falls below ion number density by more than a factor of two at z = 0.23 and 0.26 m at y = 0.7 and 0.8 m respectively. The plasma sheath thickness is affected by the Debye length of the quasi-neutral plasma and the repulsion of electrons caused by the surface. The plasma sheath thickness magnitude increases along the solar panel surface span as the surface potential drops from 0 V to -60 V in y direction for Case A as shown in Fig. 8(b). The plasma sheath thickness for Case A ranges from 0.4 to

2.5 times the local Debye length at z = 0.4 m.

The Boltzmann model is used for Case B with the same thruster exit parameters as Case A, except here the electrons are not introduced as particles at the thruster exit and the electron number density is assumed to be equal to the ion number density in the domain. An electron temperature of 2 eV is used for the Boltzmann model with $\phi_{\text{ref}} = 0$ V to compare with the inlet conditions for the kinetic model cases where $T_e = 2$ eV and $\phi = 0$ V at the thruster exit. The same surface potential as used in Case A is modelled using the superposition technique described in Sec. IIA-2. Charge and momentum exchange reactions are modeled in DSMC as in Case A with the inlet conditions shown in Tab. 2.

The kinetic case (Case A) when compared with the Boltzmann model (Case B) gives somewhat good agreement in the core plume region for the electric potential, as shown in Fig. 5(a). The electric potential for the Boltzmann model drops by about 40 V outside the core plume region because of a sudden drop in ion number density outside the plume, whereas it drops by just 7 V for the kinetic model. The reason is that the Boltzmann model assumes quasi-neutrality in the whole domain which makes the logarithm of Eq. 1 become very negative, hence decreasing the potential outside the plume region drastically. In contrast, the kinetic model has electrons present in the outside plume region which leads to a smoother transition of potential from the core plume region to the outside plume region. Thus the Boltzmann model predicts a higher radial electric field in the region outside the plume compared to the kinetic model as shown in Fig. 5(b).

The radial electric field at the plume edge is responsible for driving the slow moving ions out of the core plume region. Since the plume ions have a high axial velocity, the majority of the xenon ions present outside the plume are charge exchanged ions which have a much lower axial velocity compared to the plume ions. The normalized charge exchange (CEX) ion number density for the Boltzmann model is comparable in the core plume regions with the kinetic model but is slightly higher and more evenly spread in the backflow region as shown in Fig. 6(a). For the kinetic model, the shape of the CEX streamlines in Fig. 6(a) shows that the CEX ions have a higher radial velocity (v_y) compared to the z-velocity (v_z) which causes a very steep angle of incidence of CEX ions on the solar panel surface and a higher surface ion flux towards the edge of the solar panel surface near y = 0.0 m and y = 0.8 m. In contrast, the CEX streamlines for the Boltzmann model (Case B) are more uniformly inclined towards the surface making the surface flux more uniform compared to the kinetic case. This is because the higher y-electric field (radial electric field) extracts more charge exchange ions from the core plume for the Boltzmann model and the z-electric field, comparable to the kinetic model, results in a uniform flux on the solar panel surface. This is shown in Fig. 6(b) where the ion flux for the kinetic model (Case A) peaks towards the edge of the solar panel surface at y = 0.77 m while it is almost uniform for the Boltzmann model (Case B) along the span.

Since the surface potential varies along the span, the y coordinate of the point of incidence of the CEX ion on the surface determines the ion incidence energy. In Fig. 7(a), the ion energy distribution function (IEDF) calculated over the whole span of the solar panel surface, $0.525 < y < 0.8$ m and $0.0 < y < 0.275$ m, for the Boltzmann model (Case B) peaks at about 34 eV with a thermal spread of about 25.8 eV. The energy peak of 34 eV lies in the expected range of 0 to 60 eV for spanwise potential variation of 0 to -60 V on the surface. Since the CEX ions are uniformly incident on a surface with a 60 V potential variation, the thermal spread of 25.8 eV is higher than 10 eV which has been observed in the earlier work on ion thruster plume plasma.[3,14] With the kinetic model (Case A), however, the surface flux of CEX ions is not uniform but is much higher in the regions of the surface farther from the thruster where the surface potential with respect to the ground is -60 V. This leads to an IEDF which is not Maxwell-Boltzmann (MB) and peaks at about 63 eV as shown in Fig. 7(a). As seen in Fig. 7(a) the IEDF for the kinetic model cannot be fit by a single MB distribution because the fraction of ions incident towards the edge of the solar panel surface, $y > 0.7$ m and $y < 0.1$ m, follow a MB distribution with a peak at 63 eV and a thermal spread of 5.6 eV. The fraction of ions which incident in $0.525 < y < 0.7$ m and $0.1 < y < 0.275$ m central regions of the solar panel surface generates a secondary peak at 12 eV in the IEDF with a thermal spread of 25.8 eV as shown in Fig. 7(a).

As seen from the CEX ions streamlines in Fig. 6(a), the angle of incidence, measured with respect to the normal to the surface, is higher for the kinetic model compared to the Boltzmann model resulting in the angular distribution shown in Fig. 7(b) on the entire solar panel. The angle of incidence distribution for the kinetic model peaks at about 60^o representing the majority of CEX ions which are incident towards the edge ($y > 0.7$ m) of the solar panel surface. The angle of incidence distribution for the Boltzmann model, in contrast, shows a wider distribution and a peak at 40^o. Both the energy and angle of incidence of CEX ions play a role in estimating the surface sputtering that can be caused by these ions as was discussed in Sec. IIC. Using the PIC-DSMC simulation data in Eq. 4, the surface recession rate estimates for Cases A and B are shown in Fig. 7(c). It can be seen that the Boltzmann model predicts a higher surface recession rate by an order of magnitude compared to the kinetic model, consistent with the predicted surface flux for the Boltzmann model which is about an order of magnitude higher than the kinetic model. Therefore, the surface flux is the most dominant factor in determining the surface sputtering rate on the solar panel surface interacting with plume plasma.

The plasma sheath represents the spatial extent to which the surface affects the charged particles in its vicinity. The ions leaving radially from the plume are intercepted by the ion plasma sheath, which diverts their trajectories towards the solar panel surface. This means that the plasma sheath thickness is directly correlated to the surface ion flux. As seen Fig. 6(b), the surface flux for Case A is high towards the edge of the solar panel surface because the plasma sheath formed in front of the solar panel surface is thinner near the plume ($0.2 < y < 0.6$ m) and the radially leaving ions' trajectories are intercepted at a y location farther from the plume making most of the ions turn towards the solar panel surface farther along the span.

IV. Conclusions

In this work, we performed PIC-DSMC simulations for an ion thruster with biased solar panel surfaces in the backflow of its plume using a fully kinetic approach. We used a MPI-GPU hybrid in-house code CHAOS for this work. The Xe^+ ions, electrons and Xe atoms have a co-located source at the thruster exit where macro-particles enter with inlet conditions of the ion thruster. The results from the kinetic model cases with solar panel bias potential were compared with an equivalent Boltzmann model with same thruster and solar panel surface geometry. In the presence of biased solar panel surfaces with Dirichlet boundary condition of 0 to -60 V potential drop, the majority of xenon ions were found to be incident on the solar panel surface towards the edge. These ions had a range of 12-100 eV in incidence energy on the solar panel surface but did not follow a Maxwell-Boltzmann energy distribution. The peak energies for the IEDF for the cases, listed in Tab. 3, were found to cause a noticeable surface damage for the missions which will require a higher 10^{15} m^{-3} density ion thruster operations for 20,000 hours or longer assuming the surface flux scales linearly with the thruster exit density. The surface flux, and by extension the surface sputter rate, was found to be directly proportional to the plasma sheath thickness where the radially moving CEX ions were most influenced by the solar panel surface regions where the plasma sheath was thick. Since the number densities in the backflow region of an ion thruster plume are low enough so that the plasma sheath thickness is of the order of thruster geometry, a thin sheath approximation is not valid to study the movement of charge exchange ions towards the surfaces.

V. Acknowledgements

This work is supported by AFOSR grants AF FA9550-19-1-0164, "Experiments,Modeling and Simulation of Advanced Materials-Plasma Interactions in the Space Environment" and FA9550-16-1-0193, "Multi-Scale Characterization of Adverse Satellite Surface Conditions in a Thruster Backflow Environment". We would like to thank NCSA for providing us with the computational resources on Bluewaters petascale computing facility. We would also like to thank XSEDE for providing us with GPU computing resources on San Diego Supercomputing Cluster (SDSC).

References

[1]Goebel, D. M. and Katz, I., *Fundamentals of electric propulsion: ion and Hall thrusters*, Vol. 1, John Wiley & Sons, 2008.

[2]Van Noord, J. and Herman, D., "Application of the NEXT Ion Thruster Lifetime Assessment to Thruster Throttling," *44th AIAA/ASME/SAE/ASEE Joint Propulsion Conference & Exhibit*, 2008, p. 4526.

[3]Korkut, B., Li, Z., Levin, D., et al., "3-D Simulation of Ion Thruster Plumes Using Octree Adaptive Mesh Refinement," *IEEE,Plasma Sciences*, 2015.

[4]Sarrailh, P., Hess, S. L., Mateo-Velez, J.-C., Gineste, T., and Belhaj, M., "Simulations of plasma thruster effect on the electrostatic behavior of spacecrafts in GEO," *AIAA SPACE 2015 Conference and Exposition*, 2015, p. 4640.

[5]Roy, R., Hastings, D., and Gastonis, N., "Ion-thruster plume modeling for backflow contamination," *Journal of Spacecraft and Rockets*, Vol. 33, No. 4, 1996, pp. 525–534.

[6]Cichocki, F., Domínguez-Vázquez, A., Merino, M., and Ahedo, E., "Hybrid 3D model for the interaction of plasma thruster plumes with nearby objects," *Plasma Sources Science and Technology*, Vol. 26, No. 12, 2017, pp. 125008.

[7]Korkut, B. and Levin, D., "Three-Dimensional Simulations of Backflows from Ion Thruster Plumes Using Unstructured Grid Refinement," *Journal of Propulsion and Power*, 2016.

[8]Taccogna, F., Pagano, D., Scortecci, F., and Garulli, A., "Three-dimensional plume simulation of multi-channel thruster configuration," *Plasma Sources Science and Technology*, Vol. 23, No. 6, 2014, pp. 065034.

[9]Jambunathan, R. and Levin, D. A., "CHAOS: An octree-based PIC-DSMC code for modeling of electron kinetic properties in a plasma plume using MPI-CUDA parallelization," *Journal of Computational Physics*, Vol. 373, 2018, pp. 571–604.

[10]Wang, J., Chang, O., and Cao, Y., "Electron–ion coupling in mesothermal plasma beam emission: Full particle PIC simulations," *IEEE Transactions on Plasma Science*, Vol. 40, No. 2, 2012, pp. 230–236.

[11]Hu, Y. and Wang, J., "Electron Properties in Collisionless Mesothermal Plasma Expansion: Fully Kinetic Simulations," *Plasma Science, IEEE Transactions on*, Vol. 43, No. 9, 2015, pp. 2832–2838.

[12]Hu, Y. and Wang, J., "Fully kinetic simulations of collisionless, mesothermal plasma emission: Macroscopic plume structure and microscopic electron characteristics," *Physics of Plasmas*, Vol. 24, No. 3, 2017, pp. 033510.

[13]Usui, H., Hashimoto, A., and Miyake, Y., "Electron behavior in ion beam neutralization in electric propulsion: full particle-in-cell simulation," *Journal of Physics: Conference Series*, Vol. 454, No. 1, 2013, pp. 012017.

[14]Jambunathan, R. and Levin, D., "Kinetic, three-dimensional, PIC-DSMC simulations of ion thruster plumes, Part 1: colocated ion-electron source," *In review IEEE transactions, 2019*.

[15]Jambunathan, R. and Levin, D. A., "Advanced parallelization strategies using hybrid MPI-CUDA octree DSMC method for modeling flow through porous media," *Computers & Fluids*, Vol. 149, 2017, pp. 70–87.

[16]Serikov, V. V., Kawamoto, S., and Nanbu, K., "Particle-in-cell plus direct simulation Monte Carlo (PIC-DSMC) approach for self-consistent plasma-gas simulations," *Plasma Science, IEEE Transactions on*, Vol. 27, No. 5, 1999, pp. 1389–1398.

[17]Jambunathan, R. and Levin, D., "Self-consistent boundary condition for fully kinetic plasma plume simulations," *In review IEEE transactions, 2019*.

[18]Bird, G., *Molecular gas dynamics and the direct simulation of gas flows*, Oxford Engineering Science Series, Clarendon Press, 1994.

[19]Yamamura, Y. and Shindo, S., "An empirical formula for angular dependence of sputtering yields," *Radiation effects*, Vol. 80, No. 1-2, 1984, pp. 57–72.

[20]Bohdansky, J., "A universal relation for the sputtering yield of monatomic solids at normal ion incidence," *Nuclear Instruments and Methods in Physics Research Section B: Beam Interactions with Materials and Atoms*, Vol. 2, No. 1-3, 1984, pp. 587–591.

[21]Lai, S. T., "Fundamentals of spacecraft charging: spacecraft interactions with space plasmas," 2011.

Table 1. PIC-DSMC parameters for $N_{Xe^+} = 4 \times 10^{13}$ m^{-3} case (Case A)^{a,b}.

Species	Xe	Xe$^+$	e^-
Bulk velocity(m/s)	200	$40,000$	1
N_{dens}/N_{Xe+}	20.0	1.0	0.25
Temperature(K)	200	200	23210
Inlet type	Half-Maxwellian	12^o Gaussian beam	Half-Maxwellian
time-step(s)	5.6×10^{-6}	2.8×10^{-10}	2.8×10^{-10}
species weight	1.0	0.005	0.005

^{a} $F_{\rm num} = 3 \times 10^5$; thruster exit radii is 0.0625 m.
^{b} $\omega_{\rm pe} = 1.78 \times 10^8$ s^{-1} at thruster exit; Debye length at the thruster exit, $\lambda_{\rm D} = 0.003$ m.

Table 2. PIC-DSMC parameters for the Boltzmann model case (Case B)^{a,b}.

Species	Xe	Xe$^+$
Bulk velocity(m/s)	200	$40,000$
N_{dens}/N_{Xe+}	20.0	1.0
Temperature(K)	200	200
Inlet type	Half-Maxwellian	12^o Gaussian beam
time-step(s)	5.6×10^{-6}	2.8×10^{-8}
species weight	1.0	0.005

^{a} $F_{\rm num} = 8 \times 10^6$; thruster exit radii is 0.0625 m.
^{b} $T_e = 2$ eV; $n_{\rm e,ref} = 4 \times 10^{13}$ m^{-3} for Case B.

Table 3. Maximum surface recession rates(μm/s), S_{rec}, at peak ion energies of the ions incident on the solar panel surface for aluminum and silicon.

Case	Peak ion energy(eV)	S_{rec},aluminum
Kinetic model (A)	63.0	6.92×10^{-13}
Boltzmann model (B)	35.0	6.0×10^{-12}

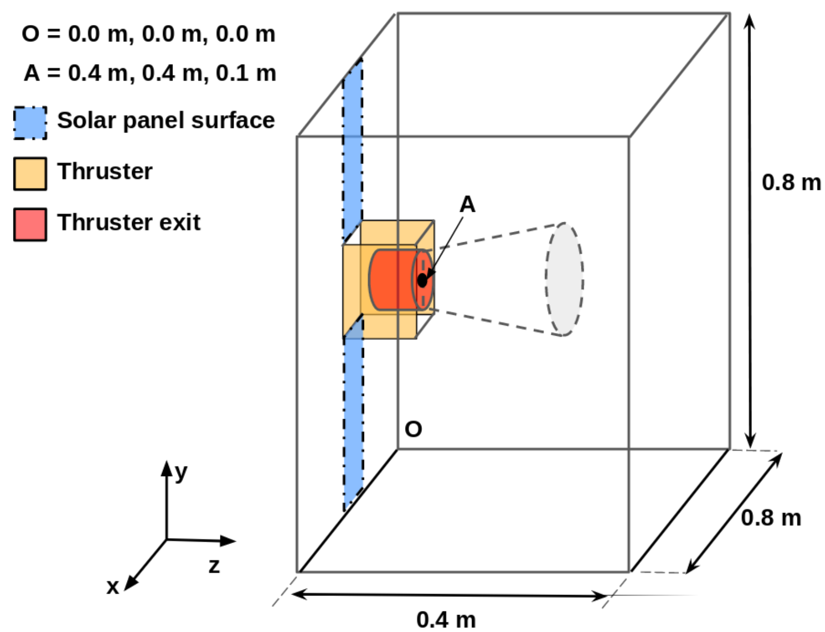

Figure 1. Schematic of computational domain. The center of circular thruster exit is marked by the point 'A' in the figure and the solar panel surface is shown in blue. The outline of the conical plume is marked in dashed lines starting from thruster exit.

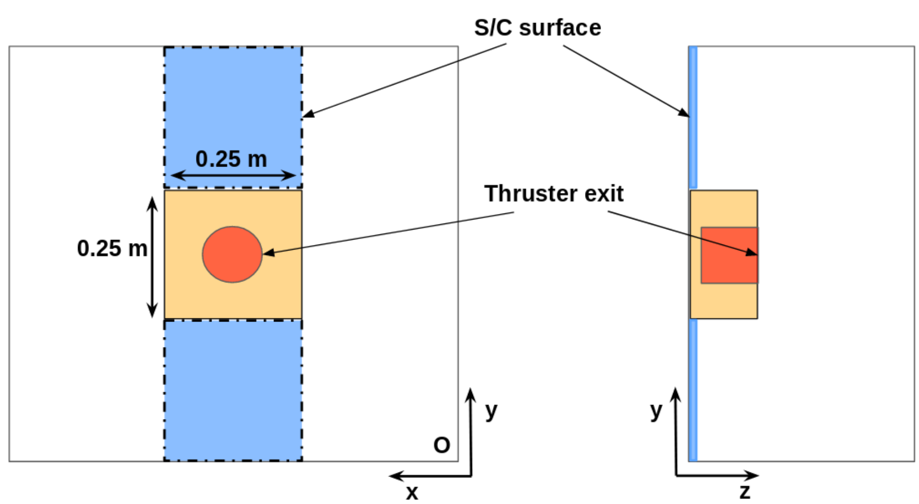

Figure 2. Sectional views of computational domain. The left figure is in a XY plane at z = 0.0 m and the right figure is in a YZ plane at x = 0.4 m.

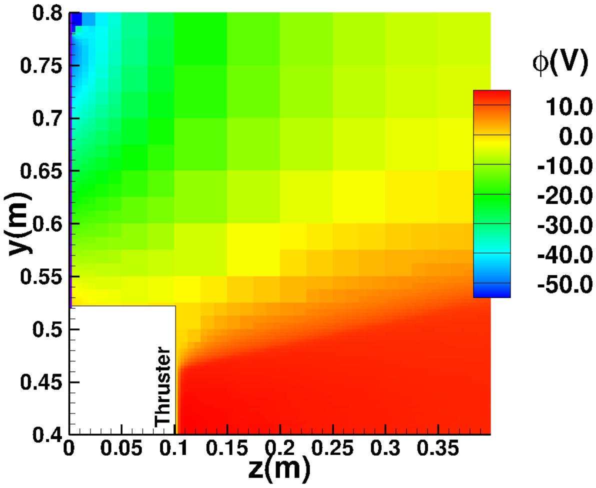

(a) Electric potential in YZ plane, at x = 0.4 m, which has the solar panel surface at z = 0.0 m.

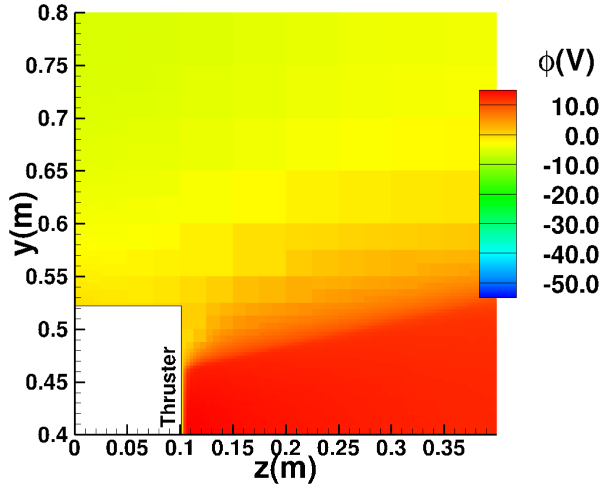

(b) Electric potential in XZ plane, at y = 0.4 m, which does not contain the solar panel surface in its backflow region.

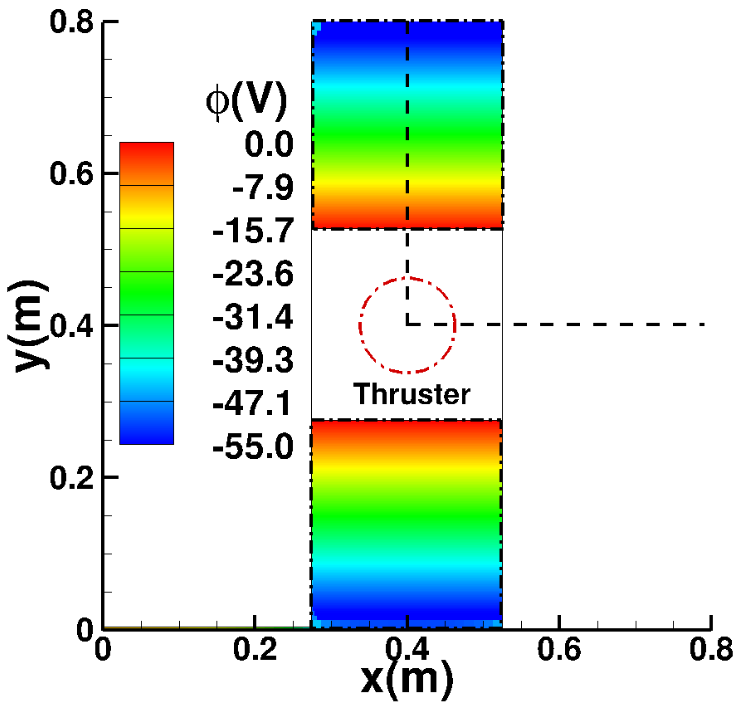

(c) Electric potential in the backflow plane, z = 0.001 m. The solar panel surface is marked by the dashed-dot black lines.

Figure 3. Electric potential at different planes for Case A. The solar panel surface has been assigned a spanwise variation of 0 V to -60 V.

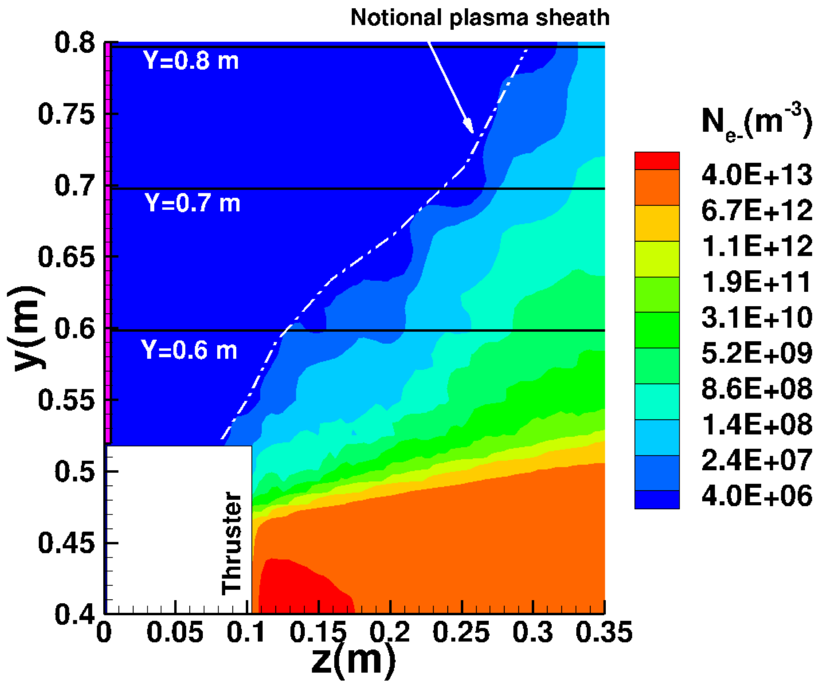

(a) Electron number density at x=0.4 m plane. A notion of ion plasma sheath is shown in white dashed-dot line.

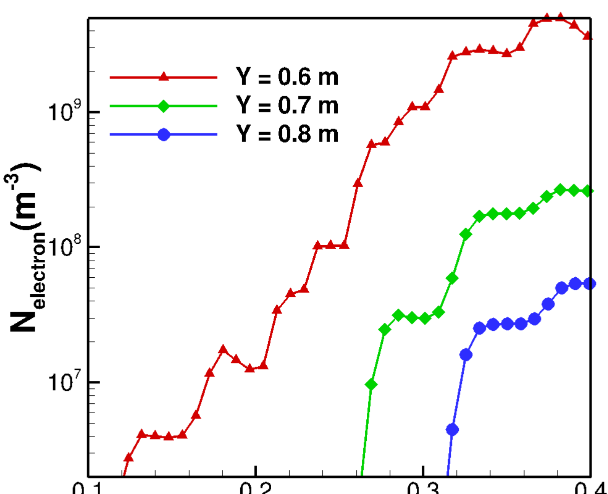

(b) Electron number densities at line probes.

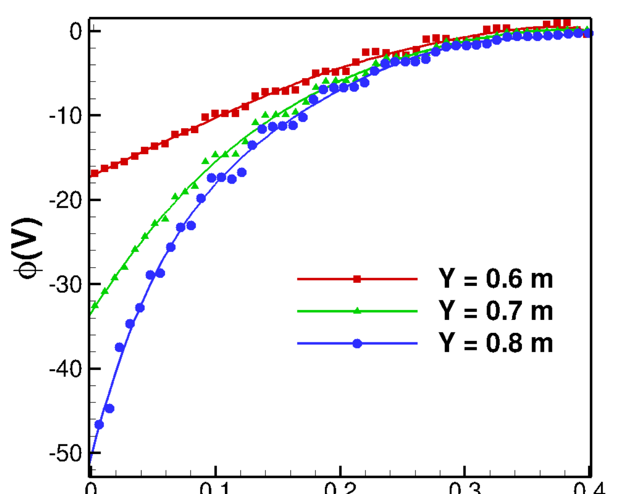

(c) Electric potential in the backflow region. The potential curves are shifted so that $\phi = 0$ V at z=0.4 m.

Figure 4. Electric potential from PIC simulation. The surface has been assigned a spanwise variation of 0 V to -60 V. The line probes show that electron number density decreases away from the plume.

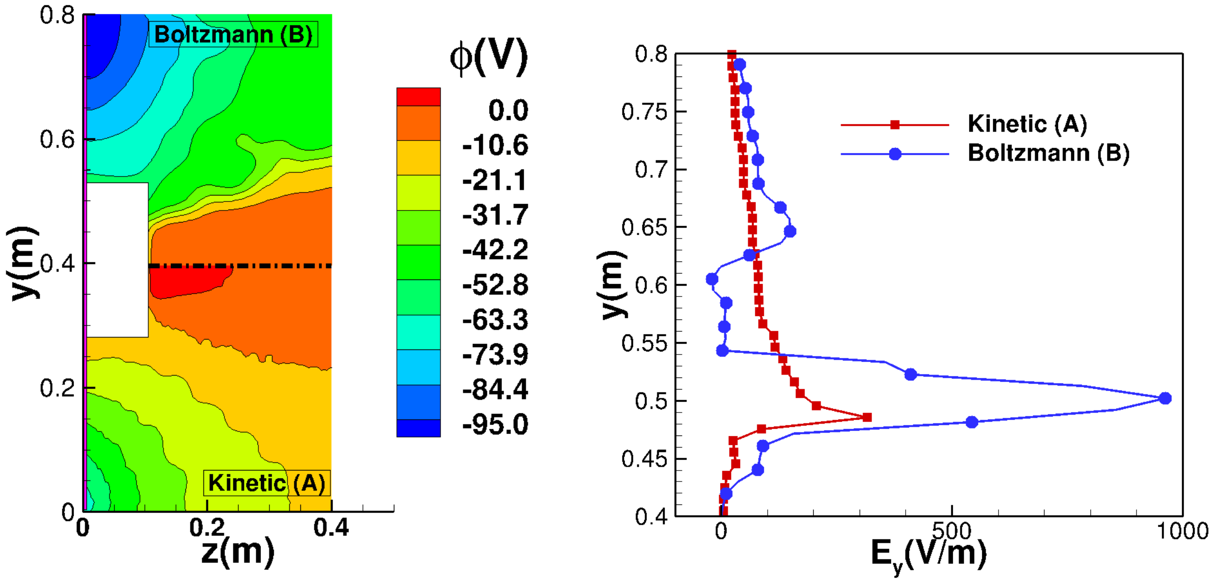

(a) Electric potential at a mid-plane.

(b) Y-Electric field along a x = 0.4 m line in the z = 0.1 m plane.

Figure 5. Comparison for results from Case A and B in a plane x=0.4 m with solar panel surfaces in the backflow region.

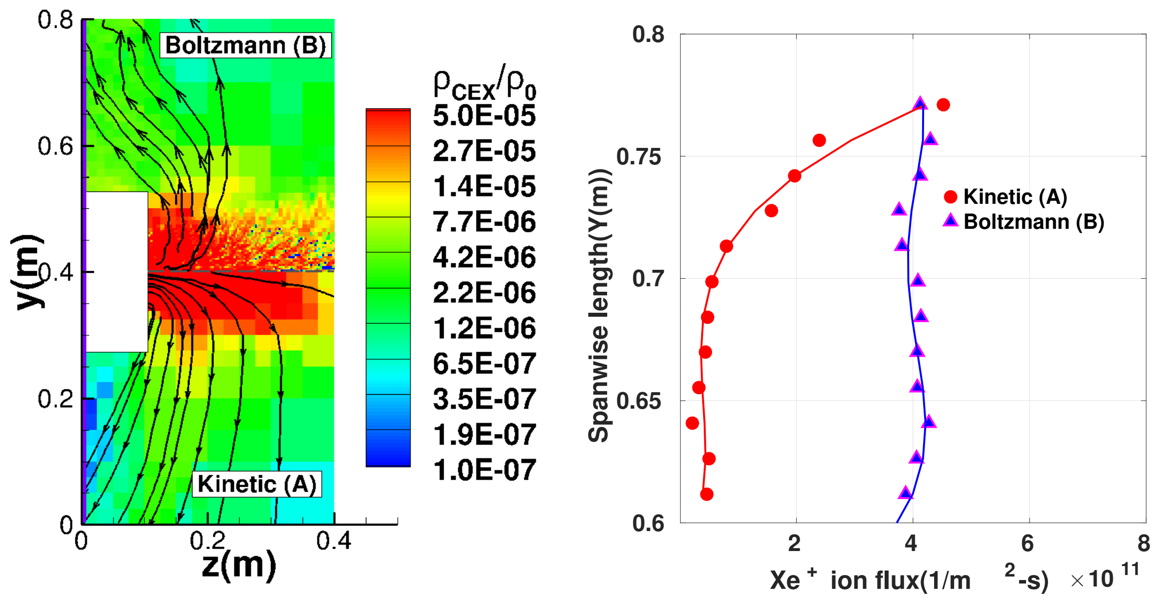

(a) CEX number density with CEX ion streamlines.

(b) Surface Xe^+ ion flux for Cases A and B.

Figure 6. A comparison of ion z-velocity and CEX density results for Cases A and B in a plane x=0.4 m. These results have solar panel surfaces in the backflow region with a spanwise variation of potential.

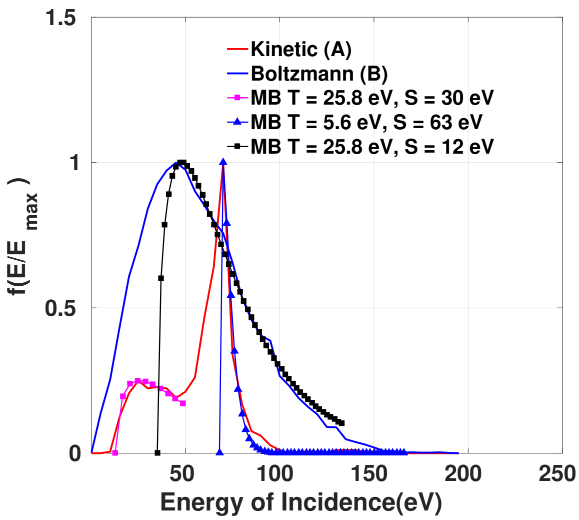

(a) IEDF of the ions incident on solar panel surface. Here ‘T’ is the fitted thermal spread and ‘S’ is shift in the MB distribution.

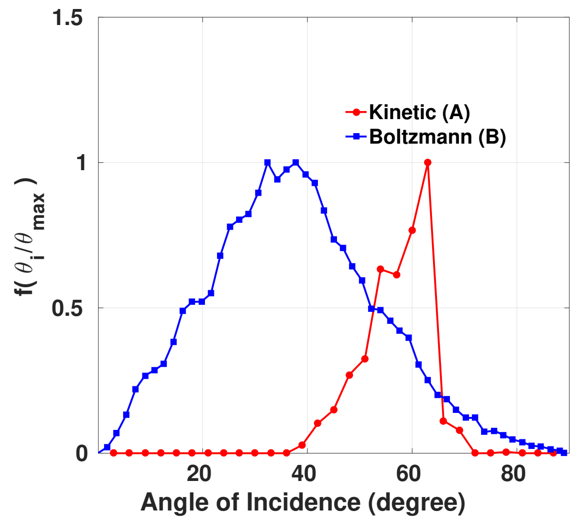

(b) Ion angle of incidence distribution of the ions incident on solar panel surface.

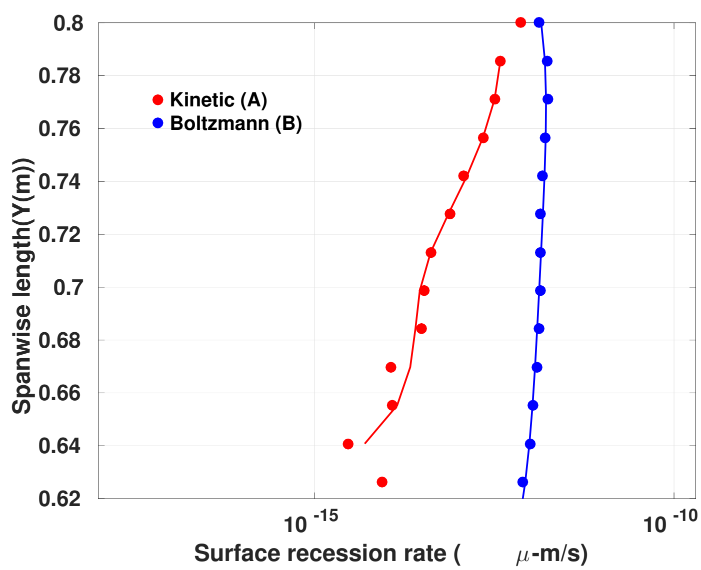

(c) Surface sputtering rate for an aluminum surface due to incidence of CEX ions on the solar panel surface.

Figure 7. Ion distribution functions and sputter rate comparison for Cases A and B.

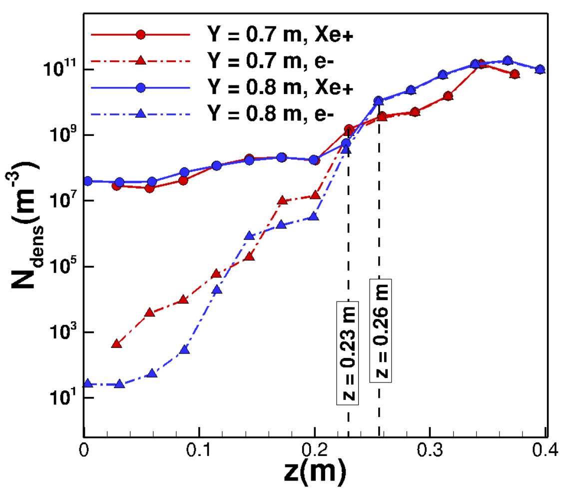

(a) Electron and ion number density in z direction at y = 0.7 and 0.8 m.

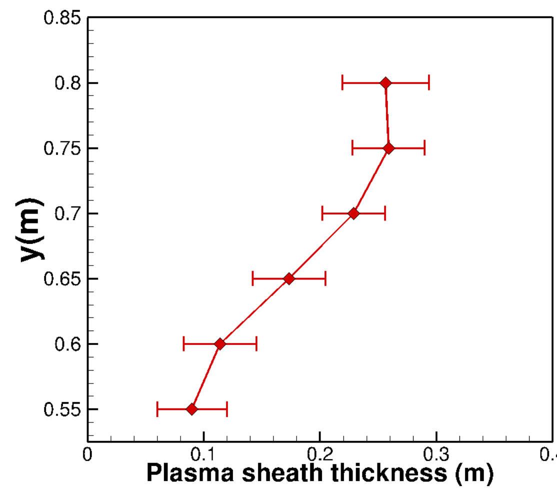

(b) Plasma sheath thickness variation along the surface span.

Figure 8. Plasma sheath thickness for the kinetic case (Case A). The error bars to the right figure represent the uncertainty in PST which is estimated by the size of the C-Octree cell where the ratio $n_i/n_e \approx 2.0$.